Distinguishing Quasiparticle-Phonon Interactions by Ultrahigh-Resolution Lifetime Measurements

Boyao Liu[,1] William Allison[,1] Bo Peng[,2] Nadav Avidor[,1] Bartomeu Monserrat,[2,3] and Andrew P. Jardine[1,*]

[1]*SMF Group, Cavendish Laboratory, University of Cambridge, 19 J J Thomson Avenue, Cambridge CB3 0HE, United Kingdom*
[2]*TCM Group, Cavendish Laboratory, University of Cambridge, 19 J J Thomson Avenue, Cambridge CB3 0HE, United Kingdom*
[3]*Department of Materials Science and Metallurgy, University of Cambridge,*
27 Charles Babbage Road, Cambridge CB3 0FS, United Kingdom

We present a determination of quasiparticle-phonon interaction strengths at surfaces through measurements of phonon spectra with ultrahigh energy resolution. The lifetimes of low energy surface phonons on a pristine Ru(0001) surface were determined over a wide range of temperatures and an analysis of the temperature dependence enables us to attribute separate contributions from electron-phonon interactions, phonon-phonon interactions, and defect-phonon interactions. Strong electron-phonon interactions are evident at all temperatures and we show they dominate over phonon-phonon interactions below 400 K.

Since the theory of quasiparticles was proposed by Lev Landau in the 1930s, it has been core to condensed matter physics, and probing interactions between quasiparticles has been a central research topic [1]. Interactions involving phonons are of particular interest. On the one hand, quasiparticle-phonon interactions play a vital role in phononics and research areas studying dissipation and propagation of phonons, such as acoustics and heat transfer [2–6]. On the other hand, interactions with phonons are also deeply involved in the research fields of other quasiparticles, such as electrons in lattices; these fields include topological surface states [7,8], electrical transport [9], superconductivity [10–14], magnonics [15], plasmonics [16,17], and the study of excitons [18]. Different approaches are used to study these interactions [19–22] and the observation of phonon linewidths [23] provides a direct measure of the interaction strength. In the case of low energy acoustic phonons, which are of interest in determining electrical and thermal properties [3], it is particularly challenging to measure linewidths and associated lifetimes directly. Here, we present measurements of acoustic surface phonon linewidths with unprecedented μeV resolution, through which quasiparticle-phonon interaction strengths can be determined.

We make use of the extreme surface sensitivity of inelastic helium atom scattering (IHAS) [24,25] to observe the surface Rayleigh mode, while achieving sufficient energy resolution to follow changes in the linewidth using the helium-3 spin echo method (HeSE) [26,27]. The method has previously been used to observe low-energy quasiparticles in reconstructed surfaces [28], and makes it possible to determine surface phonon linewidths accurately [29]. In principle, the use of helium as a probe gives access to the whole of the Brillouin zone [24], enabling us to explore phenomena beyond the reach of other high-resolution methods such as Raman spectroscopy [30–49].

As a demonstration of this technique, we study the surface phonons of ruthenium. Our experiment follows the temperature dependence of the phonon lifetime and we analyze the measurements assuming contributions from phonon-phonon and electron-phonon interactions [31,33], together with a contribution from defect scattering [50]. At room temperature, it has been generally assumed that scattering between phonons is the dominant energy dissipation mechanism limiting phonon lifetimes [3,51–57]. However, our analysis indicates that electron-phonon interactions are one of the dominant contributions to phonon lifetimes, particularly at low to moderate temperatures. These results suggest that Ru(0001) may be of particular interest to research areas in thermal and electrical transport. Moreover, the results imply that HeSE can be potentially generalized to probe systems where there are strong interactions between phonons and quasiparticles other than electrons and phonons, such as magnons and plasmons [15,16].

All the data in this work are collected by the Cambridge HeSE spectrometer in ultra high vacuum [26,58]. As indicated in Fig. 1, in a HeSE experiment a beam of spin-polarized ^{3}He atoms is produced by the ^{3}He source and polarizer. The atoms pass through the first solenoid, scatter
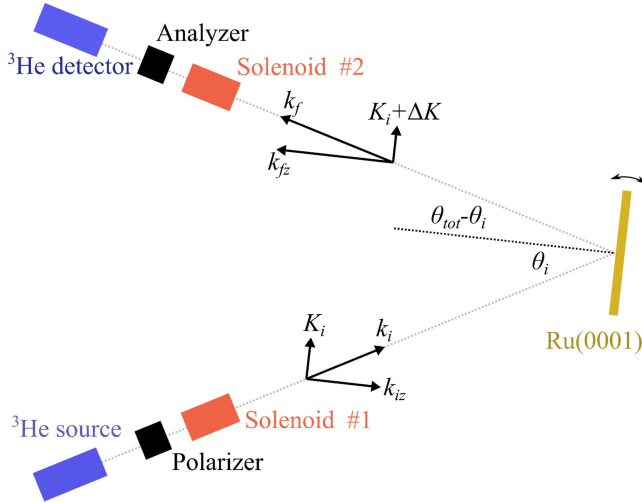
FIG. 1. A top down schematic representation of the Cambridge HeSE spectrometer. A spin-polarized supersonic ^{3}He beam is scattered from the Ru(0001) sample surface to probe surface phonons. The total scattering angle is $\theta_{\text{tot}} = 44.4°$. The angle of incidence θ_i can be varied to probe phonons with different momenta and energies.

from the surface, then traverse the second solenoid and analyzer before being detected. The nuclear spin of each ^{3}He atom undergoes Larmor precession in the two solenoids. The total precession angle is related to the velocity change during scattering, so information about the energy change of the ^{3}He atoms is encoded in the nuclear spin polarization, which is measured by the spin analyzer and detector [26]. In experiments the spin polarizations along two perpendicular directions are measured, which are denoted P_x and P_y. The currents in the two solenoids, I_1 and I_2, are varied with I_1/I_2 remaining fixed. P_x and P_y as a function of the magnitude of the current, $(I_1^2 + I_2^2)^{1/2}$, can be converted to the energy spectrum of the scattered ^{3}He beam, within which surface phonons are seen [29,59]. By rotating the sample we can change the incidence angle θ_i and measure phonons at different positions in the first Brillouin zone. Full details of the method can be found in [27,29,59] and the Supplemental Material [60].

Figures 2(a) and 2(b) show a typical dataset of spin polarizations as a a function of current magnitude. Figure 2(c) displays the energy transfer spectrum obtained from the data, together with the analysis used to extract the linewidth. We perform our analysis in the energy domain, which is sparse for single phonon scattering, whereas the time domain is not [69,70]. Thus, events with different energy transfer appear separate in the energy spectrum and are easily separable, whereas they overlap in the time domain, where the separation is more problematic. Note that the experimental resolution in the optimum tilted-scan geometry is much smaller than the linewidth, so it can be

neglected in the analysis. The line shape of the Rayleigh phonon is taken to be a Lorentzian function [71] (dotted line), while a quartic polynomial (shown dashed) represents other contributions, including the longitudinal resonance (LR) mode phonon and multiphonon scattering [72]. The goodness of the overall fit can be verified by the value of R^2, which is over 0.995 in every fit. Furthermore, the elastic peak is fitted to a Gaussian function. This Gaussian function and the Lorentzian function are transformed back into the red curves in Figs. 2(a) and 2(b), which almost overlap the experimental data and confirm the validity of the analysis. The slight deviation from the data is mainly because backgrounds around the peaks are not included when generating the curves.

The linewidth, or FWHM, of the RW phonon peak, as indicated by the red bar in Fig. 2(c), can then be extracted from every phonon spectrum. Figure 3 displays the phonon linewidths as a function of surface temperature for (a) $\theta_i = 25.825°$ and (b) $\theta_i = 28.575°$. In both cases the phonon linewidths show an initial decrease with temperature before rising at higher temperatures.

Previous studies investigated the temperature dependence of phonon linewidths in various systems, including surfaces [51–55], bulk crystals [14,30,37,39,43–47,56,73–81], 2D materials [32,34,38,82], and nanoparticles [36]. Contrary to our results, almost all of them show that linewidths of phonons increase monotonically with temperature. The only exception is a linewidth decrease with increasing temperature observed by Chae *et al.* in optical phonons of graphene [33].

Chae *et al.* used a model that includes the effects of both electron-phonon and phonon-phonon interactions to describe this phenomenon [31,33]. The phonon linewidth is expressed as $\gamma = \gamma_{\text{el−ph}} + \gamma_{\text{ph−ph}}$, where $\gamma_{\text{el−ph}}$ and $\gamma_{\text{ph−ph}}$ are the contributions from electron-phonon interactions and phonon-phonon interactions, respectively. The electron-phonon interaction can be viewed as one electron (energy E above the chemical potential) absorbing a phonon ($\hbar\omega$) to be excited to a higher energy $E + \hbar\omega$, or the reverse process of phonon creation. The contribution of those processes to the phonon linewidth is $\gamma_{\text{el−ph}} \propto f(E) - f(E + \hbar\omega)$ [33,83,84], where $f(E) = 1/[\exp(E/k_B T) + 1]$ is the Fermi-Dirac distribution. In the work by Chae and co-workers, optical phonons at the center of the first Brillouin zone were measured, so the momentum change of the electrons is close to 0. Therefore, only electrons with an energy $E = -\hbar\omega/2$ relative to the symmetric Dirac point can be excited by the phonon and reach the state with the same momentum but with an energy of $\hbar\omega/2$ above the Dirac point [33].

Since the present work studies acoustic phonons with a finite momentum and the electronic band structure in Ru(0001) is not a Dirac cone, we have to consider a range of different initial energy levels. Therefore, the contribution
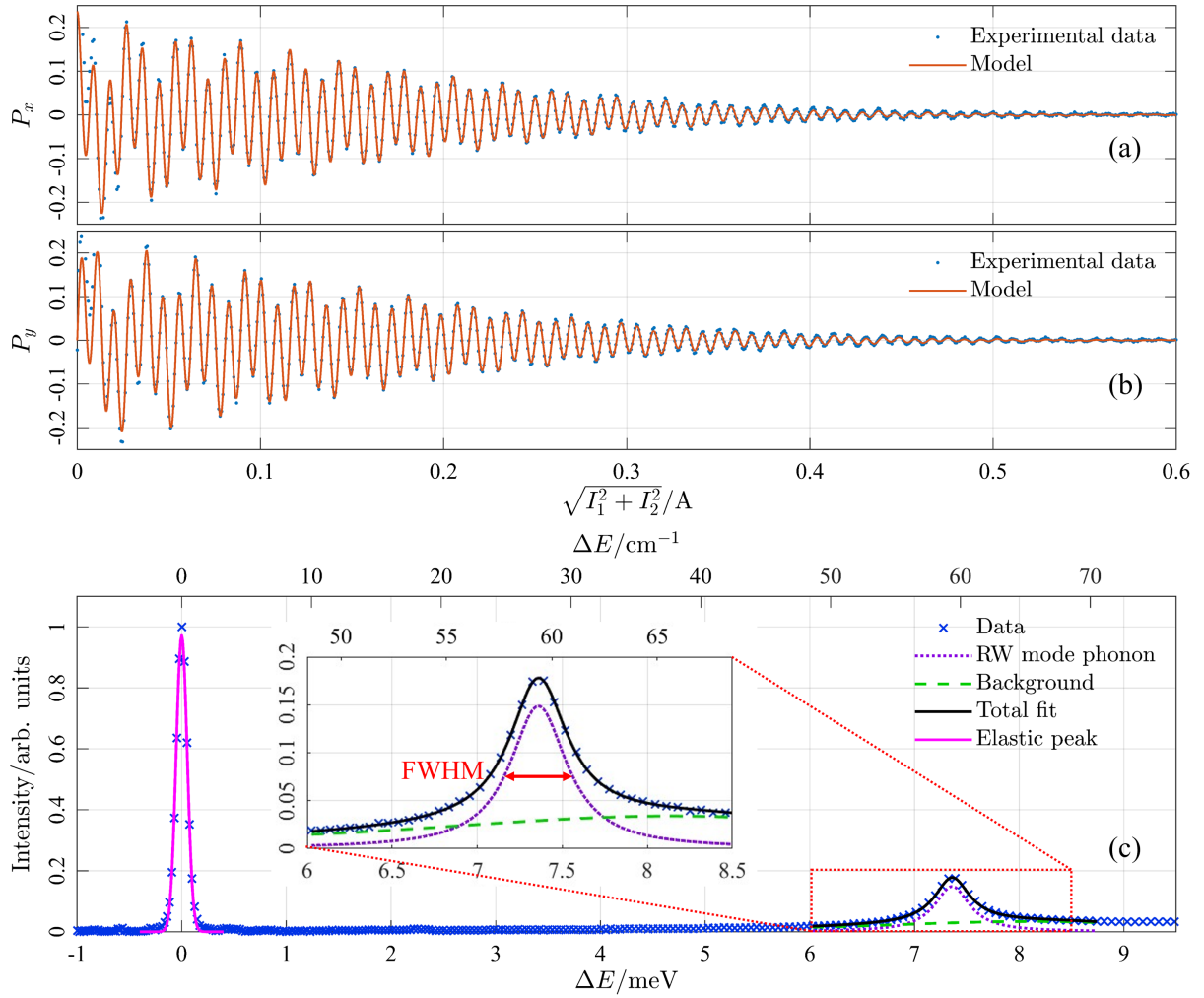
FIG. 2. (a) and (b) Raw data for the ^{3}He nuclear spin polarizations along the x and y directions as a function of current magnitude $(I_1^2 + I_2^2)^{1/2}$ are shown as blue points. The solid line is the result of a model describing the results after back transforming from the energy domain (see below). Note that the range of currents includes the complete polarization decay, which leads to the corresponding phonon spectrum. (c) The scattered intensity as a function of energy change, ΔE, of ^{3}He atoms, which is the domain where the analysis is performed. The data, blue crosses, are transformed using the method described in [27]. The RW phonon is modeled with a Lorentzian profile and the broad background is represented by a quartic polynomial. In (a) and (b), the red curves are reconverted from the elastic peak and the RW phonon peak in (c) using the reverse method. The location of the RW mode phonon peak indicates that the energy of the phonon $\hbar\omega$ is 7.4 meV. The red bar, which is the FWHM of the peak, represents the phonon linewidth, denoted γ in the text. The elastic peak around $\Delta E = 0$ is represented as a Gaussian function. The data shown correspond to a surface temperature of 625 K, an incident angle of $\theta_i = 28.575°$, and the $[1\bar{1}00]$ azimuth. The mean kinetic energy of the incoming ^{3}He atoms is 8.07 meV.

from electron-phonon interactions to the phonon linewidth is [33,83,84]

$$\gamma_{\text{el-ph}} \propto \int [f(E) - f(E + \hbar\omega)]\rho(E)\mathrm{d}E, \qquad (1)$$

where $\rho(E)$ is the weight function describing the probability that an electron with energy E undergoes the electron-phonon scattering process.

Figures 3(c) and 3(d) show $f(E) - f(E + \hbar\omega)$ at different temperatures and various values of E for the two phononic states studied in this work. It can be found that

$f(E) - f(E + \hbar\omega)$ only drops strongly as a function of temperature when 20 meV $\gtrsim E \gtrsim -20$ meV. Therefore, $\rho(E)$ is much stronger within ± 20 meV relative to the Fermi level, i.e., electrons close to the Fermi level are more likely to scatter with RW phonons than other electrons. It is this key observation which allows us to explain the reducing linewidth at low temperatures.

To investigate the origin of the enhancement in $\rho(E)$ around the Fermi level, a density functional theory (DFT) calculation was performed to evaluate the joint density of states of electrons (number of electronic states available to undergo the electron-phonon scattering process), as shown
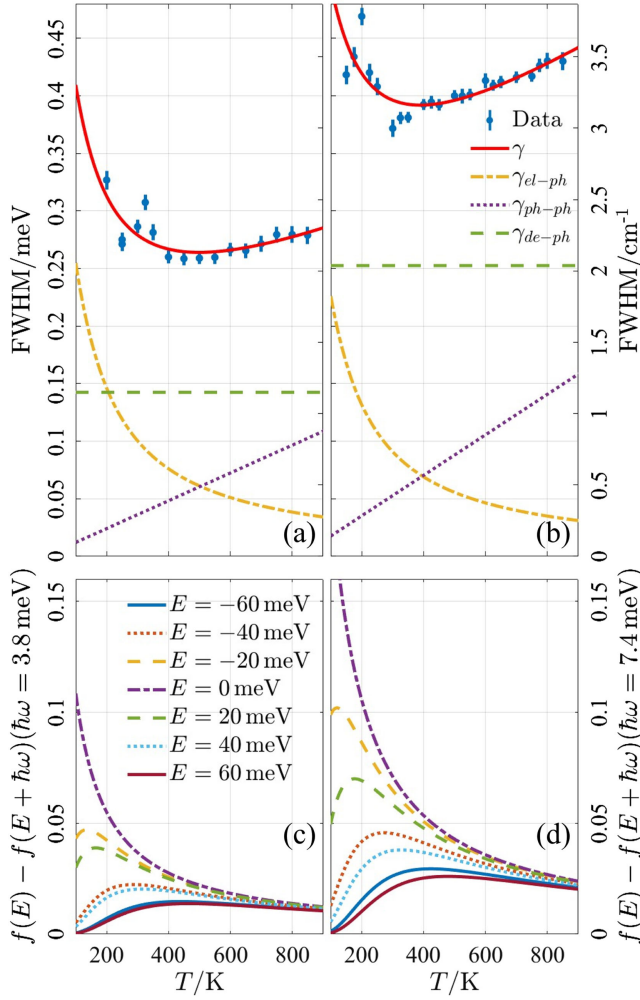
FIG. 3. (a) and (b) Temperature dependence of RW phonon linewidths along the $[1\bar{1}00]$ azimuth: (a) $\theta_i = 25.825°$ and the phonon energy is $\hbar\omega = 3.8$ meV. (b) $\theta_i = 28.575°$ and $\hbar\omega = 7.4$ meV. Blue points represent experimental data with the error bars being 95% confidence bounds in peak fitting processes illustrated in Fig. 2(b). The red solid lines represent the calculated phonon linewidth γ in Eq. (3), which can be expressed as the sum of contributions from electron-phonon interaction (yellow lines), phonon-phonon interaction (purple lines), and defect-phonon interaction (green lines). (c) and (d) $f(E) - f(E + \hbar\omega)$ as a function of temperature for various E. The values of $\hbar\omega$ correspond to the energies of phonons studied in (a) and (b), respectively.

in the Supplemental Material [60]. However, the result of the DFT calculation does not show a strong peak in the joint density of states, so some future work is still needed to fully understand why the value $\rho(E)$ is particularly large when $E \sim 0$, or whether some other mechanism is present. To proceed with the analysis in this work, we assume a simple form of $\rho(E)$ that peaks around zero,

$$\rho(E) = \begin{cases} 1 & \text{if } -\varepsilon < E < \varepsilon, \\ 0 & \text{otherwise,} \end{cases} \quad (2)$$

where ε is a factor to be determined. More precise determination of $\rho(E)$ requires further improvement on data quality.

Besides electron-phonon interaction, phonon-phonon interaction will also broaden phonon linewidths. In the temperature range studied in this work, $\gamma_{\mathrm{ph-ph}}$ is approximately proportional to the temperature of the crystal [79,82,85–87].

Beyond electron-phonon and phonon-phonon interactions, scattering from crystal defects will also shorten phonon lifetimes, and in turn, broaden phonon linewidths. This contribution depends on the defect density, which is independent of temperature in the temperature range used in this work, but is dependent on crystal qualities and the particular phononic state that is studied [50,76,77,81,82,88]. As such, a constant term $\gamma_{\mathrm{de-ph}}$ is added in the model. Combining all scattering mechanisms, we arrive at

$$\gamma = \gamma_{\mathrm{el-ph}}(\varepsilon, c_1, T) + \gamma_{\mathrm{ph-ph}}(c_2, T) + \gamma_{\mathrm{de-ph}}(c_3)$$

$$= c_1 \int [f(E) - f(E + \hbar\omega)]\rho(E)\mathrm{d}E + c_2 k_B T + c_3$$

$$= c_1 \int_{-\varepsilon}^{\varepsilon} [f(E) - f(E + \hbar\omega)]\mathrm{d}E + c_2 k_B T + c_3, \quad (3)$$

where c_1, c_2, and c_3 describe the relative strength of electron-phonon interactions, phonon-phonon interactions, and defect-phonon interactions. The parameters are fitted to the data in Fig. 3(a). The values obtained are $\varepsilon = 13.6$ meV, $c_1 = 0.1029$, $c_2 = 0.0014$, and $c_3 = 0.143$ meV. Figure 3(b) uses the same value of ε while c_1, c_2, and c_3 are varied; the results of the fit are $c_1 = 0.0481$, $c_2 = 0.00204$, and $c_3 = 0.253$ meV. While choosing a different form for $\rho(E)$ would affect the exact value of the parameters, it would not affect the key observation that a peaked form is needed.

The good quality of both fits in Fig. 3 supports our analysis of the data and demonstrates the importance of including all scattering mechanisms. At higher temperatures, phonon-phonon interaction and defect-phonon interaction are the main reason for phonon linewidth broadening. The relatively large difference in defect-phonon scattering between Figs. 3(a) and 3(b) is due to the difference in phononic modes and surface quality in the two sets of experiments. At lower temperatures, electron-phonon scattering becomes the dominant contribution to linewidths. This suggests a direct impact in research fields of thermal and electrical transport [4,9], where researchers need to choose from materials with different electron-phonon interaction strengths at various temperatures. Similarly, this phenomenon is particularly interesting in superconductivity, where electron-phonon interactions are crucial, as the results show the potential of HeSE as a new route to understand superconducting materials using IHAS [89,90].

In summary, we demonstrate that information about quasiparticle interactions in surfaces can be obtained from ultrahigh resolution linewidth measurements. This method is exemplified by the study of acoustic phonons in a Ru(0001) surface. Analysis of the experiment was performed on the basis of the expected temperature dependence of three phonon energy dissipation channels; namely, electrons, phonons, and defects. The contributions have a temperature dependence corresponding to electron-phonon scattering dominates that from phonon-phonon scattering at and below room temperature. Our method should be applicable to other quasiparticle systems accessible to HeSE, such as phasons [28]. Potential future upgrades to further improve the HeSE energy range, resolution, and temperature range, will help expand the scope for ultrahigh resolution studies of quasiparticles.

The supporting data for this work are openly available from [91].

---

*apj24@cam.ac.uk

[1] L. Venema, B. Verberck, I. Georgescu, G. Prando, E. Couderc, S. Milana, M. Maragkou, L. Persechini, G. Pacchioni, and L. Fleet, The quasiparticle zoo, Nat. Phys. **12**, 1085 (2016).

[2] M. Maldovan, Sound and heat revolutions in phononics, Nature (London) **503**, 209 (2013).

[3] P.-F. Lory *et al.*, Direct measurement of individual phonon lifetimes in the clathrate compound $Ba_{7.81}Ge_{40.67}Au_{5.33}$, Nat. Commun. **8**, 491 (2017).

[4] B. Shi, X. Tang, T. Lu, T. Nakayama, Y. Li, and J. Zhou, Interfacial thermal conductance at metal–nonmetal interface via electron-phonon coupling, Mod. Phys. Lett. B **32**, 1830004 (2018).

[5] X. Yan, C. Liu, C. A. Gadre, L. Gu, T. Aoki, T. C. Lovejoy, N. Dellby, O. L. Krivanek, D. G. Schlom, R. Wu, and X. Pan, Single-defect phonons imaged by electron microscopy, Nature (London) **589**, 65 (2021).

[6] C. A. Gadre, X. Yan, Q. Song, J. Li, L. Gu, H. Huyan, T. Aoki, S. W. Lee, G. Chen, R. Wu, and X. Pan, Nanoscale imaging of phonon dynamics by electron microscopy, Nature (London) **606**, 292 (2022).

[7] B. Peng, I. Bravić, J. L. MacManus-Driscoll, and B. Monserrat, Topological semimetallic phase in PbO_2 promoted by temperature, Phys. Rev. B **100**, 161101 (2019).

[8] B. Peng, S. Murakami, B. Monserrat, and T. Zhang, Degenerate topological line surface phonons in quasi-1D double helix crystal SnIP, npj Comput. Mater. **7**, 195 (2021).

[9] C.-H. Park, N. Bonini, T. Sohier, G. Samsonidze, B. Kozinsky, M. Calandra, F. Mauri, and N. Marzari, Electron–phonon interactions and the intrinsic electrical resistivity of graphene, Nano Lett. **14**, 1113 (2014).

[10] K. Habicht, R. Golub, F. Mezei, B. Keimer, and T. Keller, Temperature-dependent phonon lifetimes in lead investigated with neutron-resonance spin-echo spectroscopy, Phys. Rev. B **69**, 104301 (2004).

[11] G. Anemone, M. Garnica, M. Zappia, P. C. Aguilar, A. A. Taleb, C.-N. Kuo, C. S. Lue, A. Politano, G. Benedek, A. L. V. de Parga, R. Miranda, and D. Farías, Experimental determination of surface thermal expansion and electron–phonon coupling constant of 1T-$PtTe_2$, 2D Mater. **7**, 025007 (2020).

[12] P. B. Allen, Neutron spectroscopy of superconductors, Phys. Rev. B **6**, 2577 (1972).

[13] I. Y. Sklyadneva, G. Benedek, E. V. Chulkov, P. M. Echenique, R. Heid, K.-P. Bohnen, and J. P. Toennies, Mode-selected electron-phonon coupling in superconducting Pb nanofilms determined from He atom scattering, Phys. Rev. Lett. **107**, 095502 (2011).

[14] T. Keller, P. Aynajian, K. Habicht, L. Boeri, S. K. Bose, and B. Keimer, Momentum-resolved electron-phonon interaction in lead determined by neutron resonance spin-echo spectroscopy, Phys. Rev. Lett. **96**, 225501 (2006).

[15] S. Liu, A. Granados del Águila, D. Bhowmick, C. K. Gan, T. Thu Ha Do, M. A. Prosnikov, D. Sedmidubský, Z. Sofer, P. C. M. Christianen, P. Sengupta, and Q. Xiong, Direct observation of magnon-phonon strong coupling in two-dimensional antiferromagnet at high magnetic fields, Phys. Rev. Lett. **127**, 097401 (2021).

[16] E. H. Hwang, R. Sensarma, and S. Das Sarma, Plasmon-phonon coupling in graphene, Phys. Rev. B **82**, 195406 (2010).

[17] B. Diaconescu, K. Pohl, L. Vattuone, L. Savio, P. Hofmann, V. M. Silkin, J. M. Pitarke, E. V. Chulkov, P. M. Echenique, D. Farías, and M. Rocca, Low-energy acoustic plasmons at metal surfaces, Nature (London) **448**, 57 (2007).

[18] J. J. P. Thompson, D. Muth, S. Anhäuser, D. Bischof, M. Gerhard, G. Witte, and E. Malic, Singlet-exciton optics and phonon-mediated dynamics in oligoacene semiconductor crystals, Natural Sci. **3**, e20220040 (2023).

[19] A. Bostwick, T. Ohta, T. Seyller, K. Horn, and E. Rotenberg, Quasiparticle dynamics in graphene, Nat. Phys. **3**, 36 (2006).

[20] G. Baym and C. Ebner, Phonon-quasiparticle interactions in dilute solutions of He^3 in superfluid He^4: I. Phonon thermal conductivity and ultrasonic attenuation, Phys. Rev. **164**, 235 (1967).

[21] B. Liao, B. Qiu, J. Zhou, S. Huberman, K. Esfarjani, and G. Chen, Significant reduction of lattice thermal conductivity by the electron-phonon interaction in silicon with high carrier concentrations: A first-principles study, Phys. Rev. Lett. **114**, 115901 (2015).

[22] W. Yao, E. Wang, K. Deng, S. Yang, W. Wu, A. V. Fedorov, S.-K. Mo, E. F. Schwier, M. Zheng, Y. Kojima, H. Iwasawa, K. Shimada, K. Jiang, P. Yu, J. Li, and S. Zhou, Monolayer charge-neutral graphene on platinum with extremely weak electron-phonon coupling, Phys. Rev. B **92**, 115421 (2015).

[23] D. K. Ferry, Non-equilibrium longitudinal optical phonons and their lifetimes, Appl. Phys. Rev. **8**, 021324 (2021).

[24] G. Benedek and J. P. Toennies, *Atomic Scale Dynamics at Surfaces: Theory and Experimental Studies with Helium Atom Scattering*, Springer Series in Surface Sciences Vol. 63 (Springer, Berlin, Heidelberg, 2018).

[25] B. Holst, G. Alexandrowicz, N. Avidor, G. Benedek, G. Bracco, W. E. Ernst, D. Farías, A. P. Jardine, K. Lefmann, J. R. Manson, R. Marquardt, S. M. Artés, S. J. Sibener, J. W. Wells, A. Tamtögl, and W. Allison, Material properties particularly suited to be measured with helium scattering: Selected examples from 2D materials, van der Waals heterostructures, glassy materials, catalytic substrates, topological insulators and superconducting radio frequency materials, Phys. Chem. Chem. Phys. **23**, 7653 (2021).

[26] A. Jardine, H. Hedgeland, G. Alexandrowicz, W. Allison, and J. Ellis, Helium-3 spin-echo: Principles and application to dynamics at surfaces, Prog. Surf. Sci. **84**, 323 (2009).

[27] P. R. Kole, A. P. Jardine, H. Hedgeland, and G. Alexandrowicz, Measuring surface phonons with a ^{3}He spin echo spectrometer: A two-dimensional approach, J. Phys. Condens. Matter **22**, 304018 (2010).

[28] E. M. McIntosh, P. R. Kole, M. El-Batanouny, D. M. Chisnall, J. Ellis, and W. Allison, Measurement of the phason dispersion of misfit dislocations on the Au(111) surface, Phys. Rev. Lett. **110**, 086103 (2013).

[29] G. Alexandrowicz and A. P. Jardine, Helium spin-echo spectroscopy: Studying surface dynamics with ultra-high-energy resolution, J. Phys. Condens. Matter **19**, 305001 (2007).

[30] M. Kuball, J. M. Hayes, Y. Shi, and J. H. Edgar, Phonon lifetimes and decay channels in single-crystalline bulk AlN, in *Ultrafast Phenomena in Semiconductors V*, edited by H. Jiang, K.-T. F. Tsen, and J.-J. Song, International Society for Optics and Photonics Vol. 4280 (SPIE, Bellingham, WA, 2001), pp. 78–88, https://doi.org/10.1117/12.424745.

[31] M. Lazzeri, S. Piscanec, F. Mauri, A. C. Ferrari, and J. Robertson, Phonon linewidths and electron-phonon coupling in graphite and nanotubes, Phys. Rev. B **73**, 155426 (2006).

[32] S. Berciaud, M. Y. Han, K. F. Mak, L. E. Brus, P. Kim, and T. F. Heinz, Electron and optical phonon temperatures in electrically biased graphene, Phys. Rev. Lett. **104**, 227401 (2010).

[33] D.-H. Chae, B. Krauss, K. von Klitzing, and J. H. Smet, Hot phonons in an electrically biased graphene constriction, Nano Lett. **10**, 466 (2009).

[34] V. Bragaglia, M. Ramsteiner, D. Schick, J. E. Boschker, R. Mitzner, R. Calarco, and K. Holldack, Phonon anharmonicities and ultrafast dynamics in epitaxial Sb_2Te_3, Sci. Rep. **10**, 1 (2020).

[35] Y. D. Glinka, S. Babakiray, and D. Lederman, Plasmon-enhanced electron-phonon coupling in Dirac surface states of the thin-film topological insulator Bi_2Se_3, J. Appl. Phys. **118**, 135713 (2015).

[36] X. Fu, H. An, and W. Du, Temperature-dependent Raman scattering studies in ZnSe nanoparticles, Mater. Lett. **59**, 1484 (2005).

[37] L. Xu, W. Wang, Q. Xie, C. Hu, L. Chen, J. Zheng, H. Yin, G. Cheng, and X. Ai, Phonon anharmonicity in bulk $ZrTe_5$, J. Raman Spectrosc. **53**, 104 (2022).

[38] M. T. Hossain and P. K. Giri, Temperature-dependent Raman studies and thermal conductivity of direct CVD grown non-van der Waals layered Bi_2O_2Se, J. Appl. Phys. **129**, 175102 (2021).

[39] Q. Xie, L. Xu, C. Hu, L. Chen, J. Zheng, W. Wang, H. Yin, G. Cheng, and X. Ai, Phonon anharmonicity of thermoelectric material $HfTe_5$ studied by Raman spectroscopy, J. Raman Spectrosc. **52**, 988 (2021).

[40] P. Shankar, M. H. Ishak, J. K. Padarti, N. Mintcheva, S. Iwamori, S. O. Gurbatov, J. H. Lee, and S. A. Kulinich, ZnO@graphene oxide core@shell nanoparticles prepared via one-pot approach based on laser ablation in water, Appl. Surf. Sci. **531**, 147365 (2020).

[41] J. Zhang, Z. Peng, A. Soni, Y. Zhao, Y. Xiong, B. Peng, J. Wang, M. S. Dresselhaus, and Q. Xiong, Raman spectroscopy of few-quintuple layer topological insulator Bi_2Se_3 nanoplatelets, Nano Lett. **11**, 2407 (2011).

[42] B. Karthikeyan, Raman spectral probed electron–phonon coupling and phonon lifetime properties of Ni-doped CuO nanoparticles, Appl. Phys. A **127**, 1 (2021).

[43] M. Becucci, E. Castellucci, P. Foggi, S. Califano, and D. A. Dows, Temperature dependence of vibrational relaxation processes in sulfur crystals: Effect of isotopic impurities, J. Chem. Phys. **96**, 98 (1992).

[44] S. Ye, K. Tonokura, and M. Koshi, Vibron dynamics in RDX, β-HMX and Tetryl crystals, Chem. Phys. **293**, 1 (2003).

[45] J. P. Pinan, R. Ouillon, P. Ranson, M. Becucci, and S. Califano, High resolution Raman study of phonon and vibron bandwidths in isotopically pure and natural benzene crystal, J. Chem. Phys. **109**, 5469 (1998).

[46] P. Foggi and V. Schettino, Phonon relaxation in molecular crystals: Theory and experiments, La Rivista del, Nuovo Cimento (1978–1999) **15**, 1 (2007).

[47] L. Poletti, R. Bini, and V. Schettino, Vibrational relaxation of lattice phonons in CS_2 crystal, Chem. Phys. Lett. **222**, 239 (1994).

[48] B. Caldarone, C. Taiti, R. Bini, and V. Schettino, Vibrational relaxation in disordered 1,4-dihalobenzenes, J. Chem. Phys. **102**, 6653 (1998).

[49] L. Bussotti, M. Becucci, S. Califano, E. Castellucci, and D. A. Dows, Phonon dynamics and relaxation processes in

isotopically pure $^{35}Cl_2$ and natural crystalline chlorine, J. Chem. Phys. **102,** 9191 (1998).

[50] B. Liu, J. Kelsall, D. J. Ward, and A. P. Jardine, Experimental characterization of defect-induced phonon lifetime shortening, Phys. Rev. Lett. **132,** 056202 (2024).

[51] K. Kern, U. Becher, P. Zeppenfeld, G. Comsa, B. Hall, and D. L. Mills, Anharmonic linewidth broadening of surface phonons, Chem. Phys. Lett. **167,** 362 (1990).

[52] G. G. Bishop, E. S. Gillman, J. Baker, J. J. Hernández, S. A. Safron, J. G. Skofronick, S. M. Weera, and J. R. Manson, Helium-atom-scattering study of multiphonon processes on LiF(001)⟨100⟩ with temperature variation for specular and off-specular angles, Phys. Rev. B **52,** 13229 (1995).

[53] M. Gester, D. Kleinhesselink, P. Ruggerone, and J. P. Toennies, Combined helium-atom-scattering and molecular-dynamics study of aluminum surface-phonon anharmonicities and linewidths, Phys. Rev. B **49,** 5777 (1994).

[54] T. S. Rahman, J. D. Spangler, and A. Al-Rawi, Temperature variation of surface phonon line width: Low miller index surfaces of Ag and Cu, Surf. Sci. **502–503,** 429 (2002).

[55] T. S. Rahman, J. D. Spangler, and A. Al-Rawi, Theoretical studies of the surface phonon linewidth, J. Phys. Condens. Matter **14,** 5903 (2002).

[56] A. Glensk, B. Grabowski, T. Hickel, J. Neugebauer, J. Neuhaus, K. Hradil, W. Petry, and M. Leitner, Phonon lifetimes throughout the Brillouin zone at elevated temperatures from experiment and *ab initio*, Phys. Rev. Lett. **123,** 235501 (2019).

[57] A. P. Baddorf and E. W. Plummer, Enhanced surface anharmonicity observed in vibrations on Cu(110), Phys. Rev. Lett. **66,** 2770 (1991).

[58] P. Fouquet, A. P. Jardine, S. Dworski, G. Alexandrowicz, W. Allison, and J. Ellis, Thermal energy ^3He spin-echo spectrometer for ultrahigh resolution surface dynamics measurements, Rev. Sci. Instrum. **76,** 053109 (2005).

[59] G. Alexandrowicz, Helium spin echo spectroscopy: Measuring the dynamics of atoms, molecules and surfaces, Ph.D. thesis, University of Cambridge, 2005.

[60] See Supplemental Material at http://link.aps.org/supplemental/10.1103/PhysRevLett.132.176202 for additional information on the measurements and DFT calculation, which includes Refs. [61–68].

[61] J. Braun, K. Kostov, G. Witte, L. Surnev, J. Skofronick, S. Safron, and C. Wöll, Surface phonon dispersion curves for a hexagonally close packed metal surface: Ru(0001), Surf. Sci. **372,** 132 (1997).

[62] D. Maccariello, D. Campi, A. Al Taleb, G. Benedek, D. Farías, M. Bernasconi, and R. Miranda, Low-energy excitations of graphene on Ru(0001), Carbon **93,** 1 (2015).

[63] J. Kelsall, P. S. M. Townsend, J. Ellis, A. P. Jardine, and N. Avidor, Ultrafast diffusion at the onset of growth: O/Ru(0001), Phys. Rev. Lett. **126,** 155901 (2021).

[64] G. Kresse and J. Furthmüller, Efficient iterative schemes for *ab initio* total-energy calculations using a plane-wave basis set, Phys. Rev. B **54,** 11169 (1996).

[65] G. Kresse and J. Furthmüller, Efficiency of *ab-initio* total energy calculations for metals and semiconductors using a plane-wave basis set, Comput. Mater. Sci. **6,** 15 (1996).

[66] P. E. Blöchl, Projector augmented-wave method, Phys. Rev. B **50,** 17953 (1994).

[67] G. Kresse and D. Joubert, From ultrasoft pseudopotentials to the projector augmented-wave method, Phys. Rev. B **59,** 1758 (1999).

[68] J. P. Perdew, A. Ruzsinszky, G. I. Csonka, O. A. Vydrov, G. E. Scuseria, L. A. Constantin, X. Zhou, and K. Burke, Restoring the density-gradient expansion for exchange in solids and surfaces, Phys. Rev. Lett. **100,** 136406 (2008).

[69] A. Jones, A. Tamtögl, I. Calvo-Almazán, and A. Hansen, Continuous compressed sensing for surface dynamical processes with helium atom scattering, Sci. Rep. **6,** 27776 (2016).

[70] S. Maddali, I. Calvo-Almazan, J. Almer, P. Kenesei, J. S. Park, R. Harder, Y. Nashed, and S. O. Hruszkewycz, Sparse recovery of undersampled intensity patterns for coherent diffraction imaging at high x-ray energies, Sci. Rep. **8,** 4959 (2018).

[71] R. D. Mattuck, *A Guide to Feynman Diagrams in the Many-Body Problem*, 2nd ed. (McGraw-Hill, New York, London, 1976).

[72] F. Hofmann, J. P. Toennies, and J. R. Manson, A comprehensive experimental study of the dynamical interaction of He atoms with Cu(001) surface phonons, J. Chem. Phys. **101,** 10155 (1994).

[73] T. Weber, B. Roessli, C. Stock, T. Keller, K. Schmalzl, F. Bourdarot, R. Georgii, R. A. Ewings, R. S. Perry, and P. Böni, Transverse acoustic phonon anomalies at intermediate wave vectors in MgV_2O_4, Phys. Rev. B **96,** 184301 (2017).

[74] Y. P. Lai, H. J. Chen, K. H. Wu, and J. M. Liu, Temperature-dependent carrier–phonon coupling in topological insulator Bi_2Se_3, Appl. Phys. Lett. **105,** 232110 (2014).

[75] B. Schatschneider and E. L. Chronister, Temperature dependent vibrational dynamics in crystalline para-terphenyl under high pressure, Chem. Phys. Lett. **533,** 30 (2012).

[76] B. Eckert, R. Bini, H. J. Jodl, and S. Califano, High resolution infrared spectra of the ν_3 vibron in natural sulfur and in the isotopically pure ^{32}S crystal, J. Chem. Phys. **100,** 912 (1994).

[77] C. Panero, R. Bini, and V. Schettino, Vibron dynamics in naphthalene crystal, J. Chem. Phys. **100,** 7938 (1994).

[78] R. Bini and R. Spectra, High-resolution infrared study of the translational lattice modes in α-N_2 single crystals, J. Chem. Phys. **104,** 4365 (1998).

[79] R. Bini, S. Califano, B. Eckert, and H. J. Jodl, Temperature dependence of the vibrational relaxation processes in natural and isotopically pure $^{32}S_8$: Effect of the isotopic impurities on infrared phonon lifetimes, J. Chem. Phys. **106,** 511 (1998).

[80] C. Gellini, P. R. Salvi, and V. Schettino, Vibrational relaxation of multiphonon bound states in crystalline HCl, J. Chem. Phys. **106,** 6942 (1998).

[81] N. V. Surovtsev and I. N. Kupriyanov, Effect of nitrogen impurities on the Raman line width in diamond, revisited, Crystals **7** (2017).

[82] Y. Wang, H. Dai, Z. Liu, and D. Liu, Phonon scattering in monolayer molybdenum disulfide under different defect

concentrations based on temperature-dependent Raman spectra, J. Phys. Chem. C **127,** 1109 (2023).

[83] R. C. Albers, L. Bohlin, M. Roy, and J. W. Wilkins, Normal and umklapp phonon decay rates due to phonon-phonon and electron-phonon scattering in potassium at low temperatures, Phys. Rev. B **13,** 768 (1976).

[84] D. Pines, *Elementary Excitations in Solids: Lectures on Protons, Electrons, and Plasmons* (CRC Press, Boca Raton, FL, 2018), Chap. 5–5.

[85] D. G. Cahill, P. V. Braun, G. Chen, D. R. Clarke, S. Fan, K. E. Goodson, P. Keblinski, W. P. King, G. D. Mahan, A. Majumdar, H. J. Maris, S. R. Phillpot, E. Pop, and L. Shi, Nanoscale thermal transport. II. 2003-2012, Appl. Phys. Rev. **1,** 011305 (2014).

[86] I. Chatzakis, H. Yan, D. Song, S. Berciaud, and T. F. Heinz, Temperature dependence of the anharmonic decay of optical phonons in carbon nanotubes and graphite, Phys. Rev. B **83,** 205411 (2011).

[87] T. Held, I. Pfeiffer, and W. Kuhn, Theory of phonon-phonon interaction in anharmonic crystals with randomly distributed isotopic impurities, Phys. Rev. B **51,** 15027 (1995).

[88] T. Held, I. Pfeiffer, and W. Kuhn, Influence of isotopic disorder on phonon frequencies and phonon linewidths of an anharmonic crystal, Phys. Rev. B **55,** 231 (1997).

[89] G. Benedek, J. R. Manson, S. Miret-Artés, A. Ruckhofer, W. E. Ernst, A. Tamtögl, and J. P. Toennies, Measuring the electron–phonon interaction in two-dimensional superconductors with He-atom scattering, Condens. Matter Phys. **5** (2020).

[90] G. Anemone, P. Casado Aguilar, M. Garnica, F. Calleja, A. Al Taleb, C.-N. Kuo, C. S. Lue, A. Politano, A. L. Vázquez de Parga, G. Benedek, D. Farías, and R. Miranda, Electron–phonon coupling in superconducting 1T-PdTe$_2$, npj 2D Mater. Appl. **5,** 25 (2021).

[91] B. Liu, Ru(0001) surface phonon spectra, Zenodo (2024), 10.5281/zenodo.10551898.